Qiao *et al.*
Chinese Journal of Mechanical Engineering (2022) 35:87
https://doi.org/10.1186/s10033-022-00765-6

Chinese Journal of Mechanical Engineering

ORIGINAL ARTICLE

Open Access

Design and Dynamic Analysis of the Recirculating Planetary Roller Screw Mechanism

Guan Qiao[1], Rong Liao[1], Shijie Guo[1*], Zhenghong Shi[2] and Shangjun Ma[3]

Abstract

The recirculating planetary roller screw mechanism (RPRSM) is a transmission mechanism that engages the screw and nut threaded by multiple grooved rollers. In this paper, firstly, the design method of RPRSM nut threadless area is proposed, and the equations related to the structural parameters of nut threadless area are derived. On this basis, the cross-section design method of roller, screw and nut is constructed according to the actual situation of engagements between the screw/nut and the roller. By adjusting the gap between the two beveled edges and that between the arc and the beveled edge, the accuracy of the thread engagements between the screw/nut and the roller can be improved. Secondly, to ensure the engagements of the screw/nut and the roller, the distance equation from the center surface of the different rollers to the end surface of cam ring is given. Thirdly, combined with the working principle and structural composition of RPRSM, the component model is established according to its relevant structural parameters, and the virtual assembly is completed. Finally, the 3D model is imported into the ADAMS simulation software for multi-rigid body dynamics. The dynamic characteristic is analyzed, and the simulated values are compared with the theoretical values. The results show that the contact forces between the screw/nut and the roller are sinusoidal, mainly due to the existence of a small gap between the roller and the carrier. The maximum collision forces between the roller and cam ring are independent from load magnitude. Normally, the collision force between the roller and the carrier increases as the load increases. When RPRSM is in the transmission process, the roller angular speed in nut threadless area begins to appear abruptly, and the position of the maximum change is at the contact between the roller and the convex platform of cam ring. The design of the nut threadless area and the proposed virtual assembly method can provide a theoretical guidance for RPRSM research, as well as a reference for overall performance optimization.

Keywords: Recirculating planetary roller screw mechanism, Nut threadless area, Virtual assembly method, Motion relationship, Dynamic analysis

1 Introduction

The planetary roller screw mechanism (PRSM) is a new transmission mechanism that converts linear motion into rotary motion. The PRSM transmission system is quite efficient, highly reliable, and has strong bearing capacity [1, 2]. It is strategically important and promising for aero electromechanical actuation (EMA) systems [3, 4], the medical industry [5], CNC machine tools [6], and robotics [7, 8]. The recirculating planetary roller screw mechanism (RPRSM) is a common type of the PRSM used for small stroke range, limited space, and high precision applications.

A series of research on PRSM have been published internationally with focus on theoretical advancement including the design method [9], motion characteristics

*Correspondence: sjguo@imut.edu.cn

[1] Inner Mongolia Key Laboratory of Advanced Manufacturing Technology, Inner Mongolia University of Technology, Hohhot 010051, China
Full list of author information is available at the end of the article

[10], dynamics [11, 12], thermal behavior [13], and load distribution [14, 15]. However, only a few studies have been conducted on the design, kinematic characteristics, and dynamic analysis of the RPRSM, which is significantly important for EMAs in the aerospace industry.

The existing literature on PRSM design and modelling is reported as below. Ma et al. [16] summarized the design conditions of the basic structural parameters to satisfy the motion principle of PRSM. The matching combination of the number of thread heads, the number of rollers and the structural parameters of the thread is covered in their study. Lisowski et al. [17, 18] proposed a design method for the meshing part of the gear in PRSM. The rational design helps to reduce the sliding between the roller-screw/nut thread meshing surfaces, and the root size of the roller thread profile was optimized by finite element calculation from the perspective of contact stress reduction. Shih et al. [19] established a finite element model to analyze the deformation and stress-strain of the PRSM during the working process, to obtain the optimal structural parameters, and to derive a method to improve the surface quality of the parts. Ma et al. [20] studied the optimization design and contact analysis of PRSM, and half of the thread angle and the tooth thickness of the pitch circle diameter are used as the optimal variables to minimize the meshing gap of the thread pair. Abevi et al. [21] used finite element method to describe the static behavior of the inverted PRSM system under heavy load. A sectorial model of the mechanism was built involving an entire roller to show the state of the contacts and the in-depth stress zones.

In the area of kinematic characteristics and dynamic analysis of PRSM, Fu et al. [22] proposed a two-nut PRSM dynamics model considering elastic deformation, and verified the accuracy of the model by comparing its dynamic characteristics and the load distribution between threads with published literature. Fu et al. [23] also proposed a kinematic model of PRSM considering the position error and runout error. Ma et al. [24] studied the differential principle of thread transmission, and an analytical model considering helical directions between screw and roller threads in PRSM was presented in this work. Qiao et al. [25] established a mathematical model of electromechanical actuator based on PRSM, and discussed the influence of nonlinear factors such as structural stiffness, friction and clearance on the dynamic performance of the transmission system. Jones et al. [26] built a kinematic model to predict the axial migration of the rollers with respect to the nut. It is discovered that roller migration is due to slip at the nut side, which is caused by a pitch mismatching between the spur-ring gear and effective nut-roller helical gear pair. The results also indicate that the roller migration does not affect the overall lead of the PRSM. Hojjat et al. [27] found that the main factor influencing the PRSM transmission lead was the change in contact position. Ma et al. [28] established the dynamic characteristic analysis model of PRSM by considering the effects of drive clearance, friction, thread tooth contact deformation and machining error. At present, there are few related studies on RPRSM, and the available references do not cover the study of RPRSM dynamics analysis. There's also few virtual prototype technologies to demonstrate the angular speed, contact force and collision force variations of its main components.

Based on the working principle and structure composition of RPRSM, the design method of screw, roller, nut, cam ring and carrier is proposed in this paper. The correlation equation of structural parameters of nut threadless area is deduced. The relevant size parameters and design contours of thread teeth are given. The three-dimensional modeling and virtual assembly are carried out according to the structural parameters. At the same time, the RPRSM motion relationship is theoretically analyzed, and the equations are derived. The dynamic simulation results are compared to the analytical values to verify the correctness of the simulation.

2 Main Parts Design

As shown in Figure 1, the RPRSM consists of cam ring, nut, roller, screw, carrier and other auxiliary parts. Among them, the nut and the screw have the same pitch. They are single threaded, and the thread tooth profile is usually triangular. The roller is grooved without helix angle, and the thread tooth cross-section profile is circular. The carrier has a number of uniformly distributed straight grooves to hold rollers along the axial circumference of the screw.

The RPRSM transmits motion by multiple rollers from the driving screw, and the rollers drive the nut for linear motion. The rollers both rotate around their own axes and perform circular motion around the screw. When

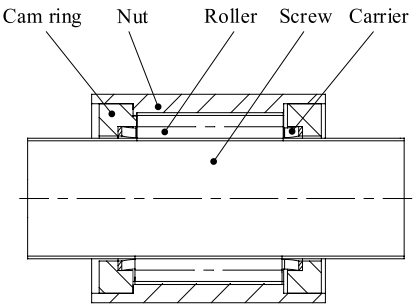

Figure 1 RPRSM Structure

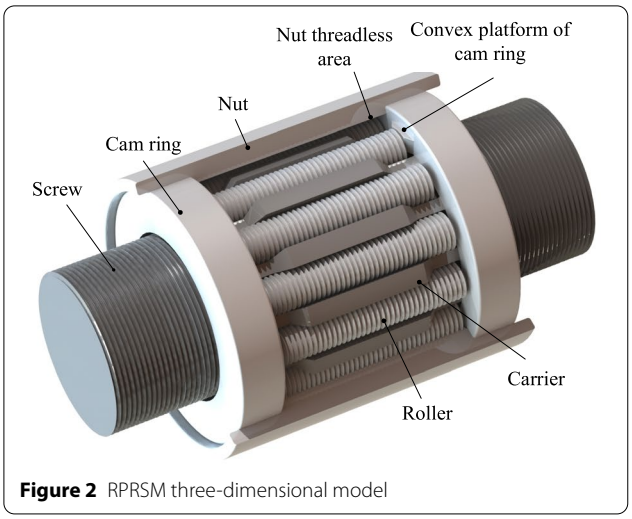

Figure 2 RPRSM three-dimensional model

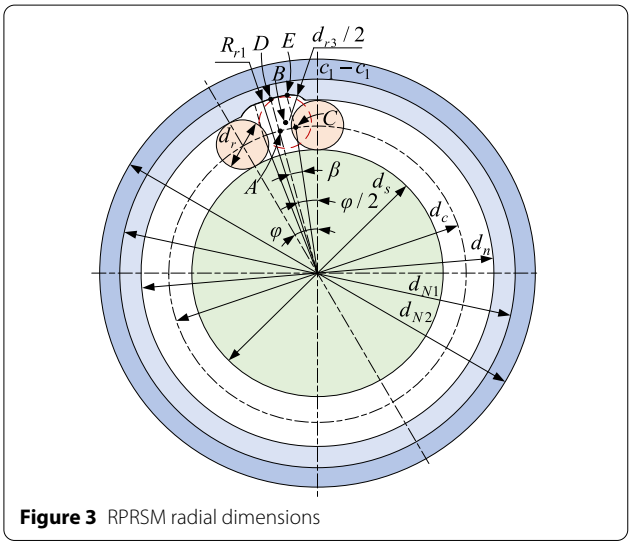

Figure 3 RPRSM radial dimensions

the screw is used as a reference, the roller moves in the same direction as the nut. The special situation is that when the nut is a reference, the roller completes the circumferential motion along the nut raceway and moves in one direction, and then enters the nut threadless area, that is, completes the reset action by the convex platform of cam ring. Its axial movement direction is opposite to the previous one. Its three-dimensional model is shown in Figure 2.

2.1 Design of Three Main Parts

The thread profile of the screw and nut is triangular, in which the nut has a threadless area at a certain angle in the circumferential direction. According to the structure and working principle of RPRSM, its radial dimension diagram is shown in Figure 3, where point A is the center point of the roller and indicates the beginning of roller disengagement with the screw. Point B is the center point of the roller and indicates the highest position of radial movement, and point C is also the center point of the roller and indicates the re-engagement of the roller with the screw. Point D is the position corresponding to point A radially in the nut threadless area, and point E is the position corresponding to point C radially in the nut threadless area.

In the radial direction, the screw, rollers and nut must meet the concentric conditions:

$$d_n = d_s + 2d_r, \tag{1}$$

where d_s is the pitch diameter of the screw, d_r is the pitch diameter of the roller, and d_n is the pitch diameter of the nut internal thread.

The screw and the nut have the same helical direction and number of heads, and the pitch is also equal, that is:

$$n_s = n_n, \tag{2}$$

$$p_s = p_n, \tag{3}$$

where n_s is the number of screw heads, n_n is the number of nut heads, p_s is the screw pitch, and p_n is the nut pitch.

Since the head number and pitch of the screw and the nut are the same, their pitch diameters are distinctly different, so their helix angles are not the same, and the screw helix angle ψ_s is larger than the nut helix angle ψ_n:

$$\psi_s = \arctan\frac{n_s p_s}{\pi d_s} > \psi_n = \arctan\frac{n_n p_n}{\pi d_n}. \tag{4}$$

In order to ensure that the contacts between the roller and the screw/nut are point contact, the roller thread contour surface adopts the arc surface, and the radius of the arc R_{r2} is expressed as:

$$R_{r2} = \frac{d_r}{2\sin\frac{\alpha}{2}}, \tag{5}$$

where α is the tooth angle of roller.

As shown in Figure 3, the motion curve of the roller barycenter can be known from the beginning of the roller crossing the thread teeth of the screw under the action of the convex platform of cam ring to the roller engagement with the screw. The trajectory is drawn in Figure 4. The distance of the z-axis p_s corresponds to the height of the convex platform of cam ring and the z-axis coincides with the center axis of the roller. Point A is the same as that in Figure 3, point A' is the position of the maximum radial height when the roller crosses the thread teeth of the screw, and point A'' is the position of the normal engagement between the roller and the screw after the reset.

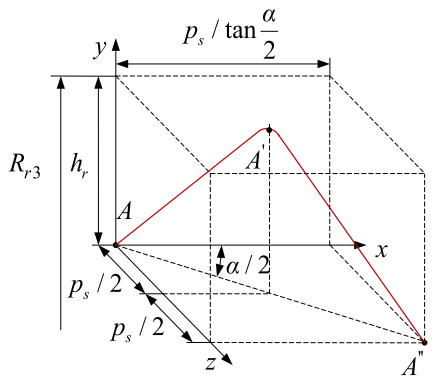

Figure 4 Motion curve of roller barycenter

As shown in Figure 4, point A is the center point of the roller, so R_{r3} can be expressed as:

$$R_{r3} = \frac{d_r}{2} + \frac{d_s}{2} + h_r, \tag{6}$$

where R_{r3} is the distance to the center axis of the screw when the roller barycenter moves radially to the highest point A'.

The maximum height h_r of radial movement of the roller barycenter is:

$$h_r = \frac{d_{r3} - d_r}{2} + \frac{d_{s3} - d_s}{2}, \tag{7}$$

where d_{r3} is the major diameter of the roller, and d_{s3} is the major diameter of the screw.

Combining this with Eqs. (6) and (7), as well as the structural relationship among the roller, screw and nut, we have the following expression about the radius R_{r1} of the nut threadless area:

$$R_{r1} = \frac{d_s}{2} + d_r + \frac{d_{r3} - d_r}{2} + h_r, \tag{8}$$

As shown in Figure 3, the nut threadless area is divided into three arcs circumferentially: the first arc radius being $d_{r3}/2$, the second arc radius being R_{r1}, and the third arc radius being $d_{r3}/2$. From Figures 3 and 4, we know that the projection trajectory from point A to point A'' on x-axis corresponds to the nut threadless area $\overset{\frown}{DE}$. Therefore, the arc $\overset{\frown}{DE}$ is equal to the ratio of the screw pitch to the tangent of one-half tooth angle, and the ratio of the arc $\overset{\frown}{DE}$ to the circumference of roller revolution is equal to the ratio of β to 360°, that is:

$$\overset{\frown}{DE} = \frac{p_s}{\tan\frac{\alpha}{2}}, \tag{9}$$

$$\frac{\overset{\frown}{DE}}{\pi d_c} = \frac{\beta}{360^\circ}, \tag{10}$$

where β is the orbital angle of the roller across the screw thread, d_c is the orbital diameter of the roller, $\alpha/2$ is the chamfer of the roller in contact with the convex platform of cam ring.

Combining Eqs. (9) and (10), one can obtain:

$$\beta = \frac{p_s 360^\circ}{\pi d_c \tan\frac{\alpha}{2}}. \tag{11}$$

Generally, RPRSM needs to be operated in forward rotation and reverse rotation, so the angle corresponding to the nut threadless area is 2β. The rollers rotate in the screw and nut raceway, and they are separated by the carrier. Each roller maintains the same angular distance, and the angle between the rollers is:

$$\varphi = \frac{360^\circ}{N}, \tag{12}$$

where φ is the angle between the rollers, and N is the number of rollers.

As can be seen from Figure 2, the orbital angle of the roller across the screw thread is less than one-half of the angle between the rollers, that is:

$$\beta < \frac{\varphi}{2}. \tag{13}$$

Combining Eqs. (12) and (13) yields:

$$N < \frac{\pi d_c \tan\frac{\alpha}{2}}{p_s}. \tag{14}$$

From Eq. (14), it can be seen that the number of rollers is influenced by the pitch p_s, the orbital diameter of the roller d_c and the tooth angle α.

2.2 Design of Carrier

The carrier is designed for straight groove, which semicircle diameter and major diameter of roller is the same. The structure schematic diagram is shown in Figure 5.

The carrier needs to rotate inside the nut, so the external diameter of the carrier D_B is smaller than the minor diameter of the nut d_{n1}, and is greater than the sum of the major diameter of the screw d_{s3} and the minor diameter of the roller d_{r1}, that is:

$$d_{s3} + d_{r1} < D_B < d_{n1}. \tag{15}$$

Meanwhile, the internal diameter of the carrier d_b must be larger than the major diameter of the screw:

$$d_b > d_{s3}. \tag{16}$$

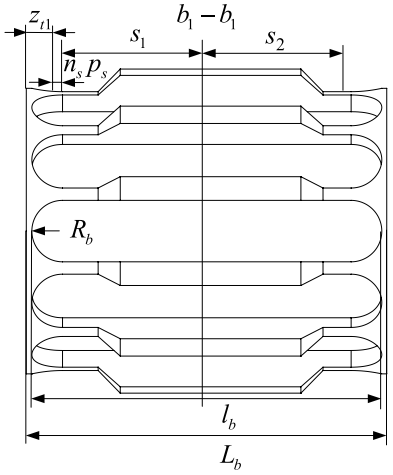

(a) Main view of carrier

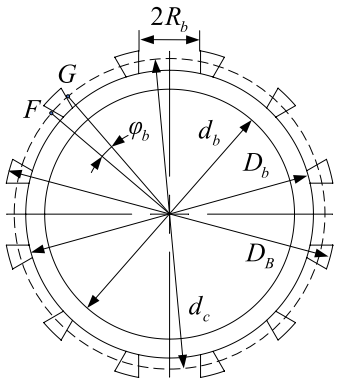

(b) Right view of carrier

Figure 5 Schematic diagram of carrier

In order to ensure that the roller can move in axial direction properly in the carrier, the length of the straight groove should be:

$$l_b = 2R_b + 2n_s p_s + s_1 + s_2, \tag{17}$$

where l_b is the straight groove length of the carrier, s_1 and s_2 are the half of roller length, R_b is the radius of the arc at both ends of the straight groove.

The major diameter of the roller d_{r3} and the arc radius of the straight groove have the relationship of:

$$d_{r3} = 2R_b. \tag{18}$$

To virtually assemble the RPRSM, one needs to establish the carrier reference plane $b_1 - b_1$ which is parallel to the carrier end surface. The specific location is $z_{t1} + n_s p_s + s_1$ away from the left end face as shown in Figure 4(a) and z_{t1} is cam ring step thickness. Taking the plane $b_1 - b_1$ as a reference, plane $b_2 - b_2$ that is p_s/N away from the left end surface of the carrier in Figure 5 can be built, and then other $N - 2$ planes are set at the same distance accordingly.

2.3 Design of Cam Ring

According to the working principle of cam ring, the end surface is shown in Figure 6. In order to ensure that the roller can be reset properly, the chamfer of the convex platform should be one-half of the roller tooth angle, that is $\alpha/2$, and the convex platform of cam ring thickness should be one lead of $n_s p_s$, as shown in Figure 7.

The convex platform of cam ring plays an important role in the RPRSM transmission process, which is similar to the circulating device of the ball screw mechanism [29] and allows the rolling body to reset. The cam ring is assembled coaxially with the screw, carrier and nut, and its inner diameter d_t should be larger than the major diameter of the screw d_{s3}:

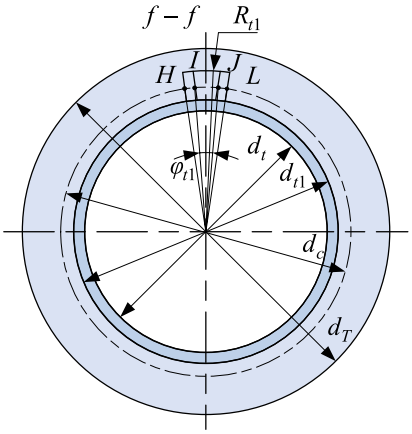

Figure 6 End surface of cam ring

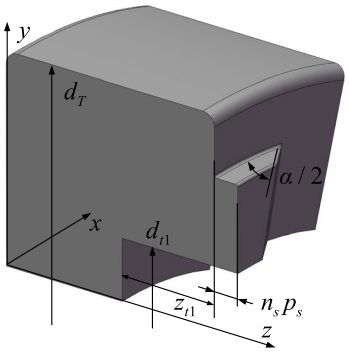

Figure 7 Partial enlargement of the convex platform of cam ring

$$d_t > d_{s3}. \tag{19}$$

The internal diameter of convex platform d_{t1} should be the same as the carrier external diameter D_b:

$$d_{t1} = D_b. \tag{20}$$

The radius of the outer surface of the convex platform R_{t1} is less than the half of the nut minor diameter d_{n1}:

$$R_{t1} < d_{n1}/2. \tag{21}$$

As one can see from Figures 5 and 6, the center angle φ_b corresponding to the carrier arc $\widehat{FG}$ is equal to the center angle φ_{t1} corresponding to cam ring arc $\widehat{IJ}$:

$$\varphi_b = \varphi_{t1}. \tag{22}$$

2.4 RPRSM Motion Analysis

According to the working principle of RPRSM, its motion sketch is shown in Figure 8. Point P is the starting position of a roller contacting with the screw, point Q is the end position of the roller after one screw rotation, φ_c is the angle of roller rotation in between, ω_s is the angular speed of the screw, ω_c is the angular speed of carrier or roller rotation, ω_r is the angular speed of roller spin.

Since the nut is fixed circumferentially and the screw is fixed axially, the point M is the instantaneous center of absolute velocity, and the absolute velocity v_O at point O is:

$$v_O = \frac{v_P}{2} = \frac{\omega_s d_s}{4}. \tag{23}$$

Also, the velocity at that point O can be expressed as:

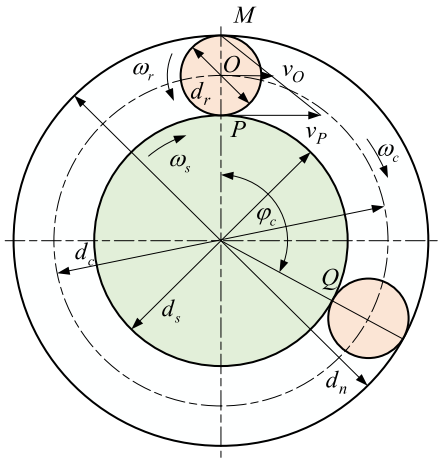

Figure 8 RPRSM motion diagram

$$v_O = \frac{\omega_c d_c}{2}. \tag{24}$$

Therefore, the union of Eqs. (23) and (24) results in:

$$\omega_c = \pm\frac{d_s}{2d_c}\omega_s = \pm\frac{(d_n - 2d_r)}{2(d_n - d_r)}\omega_s, \tag{25}$$

where the ± sign indicates that the direction of rotation, clockwise rotation is positive and counterclockwise rotation is negative.

According to Figure 8, RPRSM satisfies the ratio equation of turnover wheel train:

$$i_{sr}^H = \frac{\omega_s - \omega_c}{\omega_r - \omega_c} = -\frac{d_r}{d_s}, \tag{26}$$

$$\omega_r = \pm\left[\left(\frac{d_s}{d_r} + 1\right)\omega_c - \frac{d_s}{d_r}\omega_s\right], \tag{27}$$

where i_{sr}^H is the transmission ratio between the screw and the roller in the conversion wheel system; ± sign indicates that the direction of rotation; clockwise rotation is the positive value; counterclockwise rotation is the negative value.

The axial movement displacement L_n of the nut with respect to the screw is:

$$L_n = \pm\frac{np\omega_s t}{2\pi}. \tag{28}$$

Therefore, the axial movement velocity v_n of the nut with respect to the screw is:

$$v_n = \pm\frac{np\omega_s}{2\pi}, \tag{29}$$

where n is the number of heads of the screw or nut; p is the pitch of the screw or nut; t is the time; ± sign is decided according to the right-hand rule. When the screw is in clockwise rotation, Eqs. (28) and (29) should take "+", and when the screw is in counterclockwise rotation, Eqs. (28) and (29) should take "−".

According to the principle of RPRSM motion, the angle of roller rotation is:

$$\varphi_c = \frac{\omega_c}{\omega_s}\varphi_s, \tag{30}$$

where φ_s is the angle that the screw has turned.

The roller displacement L_{r1} with respect to the nut is:

$$L_{r1} = \frac{p}{2\pi}\varphi_c. \tag{31}$$

The displacement L_{r2} of the roller in the threaded area of the nut with respect to the screw is:

Table 1 Main structural parameters of components

Parameter	Screw	Roller	Nut
Major diameter(mm)	32.68	8.18	47.80
Pitch diameter(mm)	32	7.5	47
Minor diameter(mm)	31.20	6.70	46.32
Number of heads	1	–	1
Rotation	Right-handed	–	Right-handed
Number	1	12	1
Thread angle(°)	60	60	60
Helix angle(°)	0.57	–	0.39
Pitch(mm)	1	–	1
Groove spacing(mm)	–	1	–
Thread length(mm)	100	–	40.08

$$L_{r2} = L_n - L_{r1}. \tag{32}$$

The displacement L_{r3} of the roller with respect to the screw is:

$$L_{r3} = L_{r2} + p. \tag{33}$$

Eqs. (30)–(33) analyze the displacement magnitude of the roller relative to different reference objects, which can understand the roller motion more clearly and compare with the simulation results to verify the correctness.

3 RPRSM Virtual Modeling and Assembly Method

3.1 RPRSM Virtual Modeling

Taking a common size RPRSM as an example, its relevant parameters are listed in Table 1, and a three-dimensional model can be established according to the parameters.

Both the screw and the nut use a scan cut feature to generate the thread tooth, with the scan path being a spiral and starting at the intersection of the midline of the cut profile and the pitch diameter. The scanning profile is triangular and lies on the reference plane passing through the central axis of the part. Also, since the contacts between the screw/nut and the roller are point contact and the working surface is the thread tooth, the beveled edges of the scanning profile of the screw and nut are set to be straight. As shown in Figures 9 and 10, the scanning profile of the screw and the nut can be determined from the structural parameters in Table 1.

The roller tooth is grooved, so the modeling only requires a rotational removal and a linear array corresponding to the number of thread teeth. The roller scanning profile is subtriangular and located on the reference plane passing through the central axis of the roller. As plotted in Figure 11 based on structural parameters in Table 1, the beveled edge of the scanning profile of the roller is set to be curved.

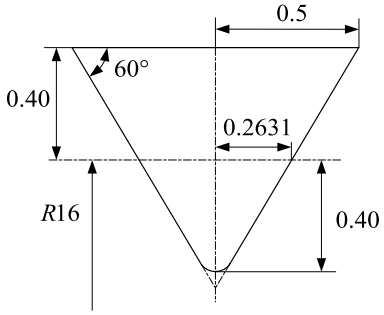

Figure 9 Scanning profile of screw removal

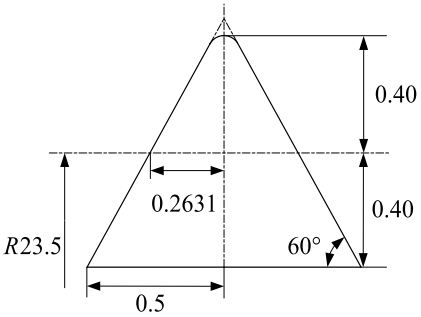

Figure 10 Scanning profile of nut removal

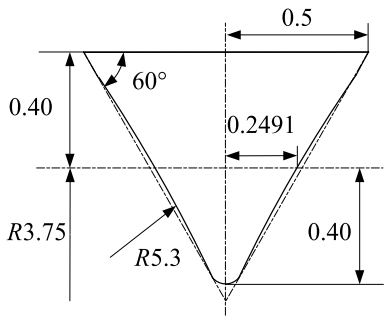

Figure 11 Rotational removal profile of roller

According to the theory of engagement, there is a certain clearance between the screw/nut and the roller, as shown in Figure 12 for the cross-section of roller-nut engagement and Figure 13 for the roller-screw engagement. The engagement point can be obtained by turning a certain angle around the central axis.

As one can see from Figures 12 and 13, the beveled edge of the roller triangular is parallel to that of the screw/nut, and moving the triangle radially can change the gap between the two edges. The actual contacts between the screw/nut and the roller are the contacts between the roller arc and the beveled edge of the screw/

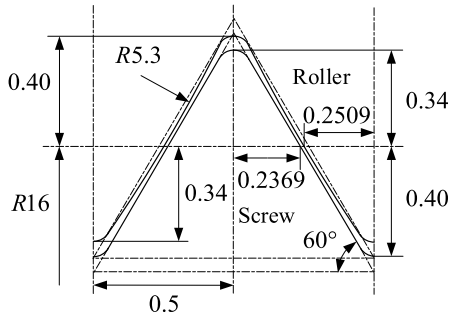

Figure 12 Cross-sectional view of the screw-roller engagement

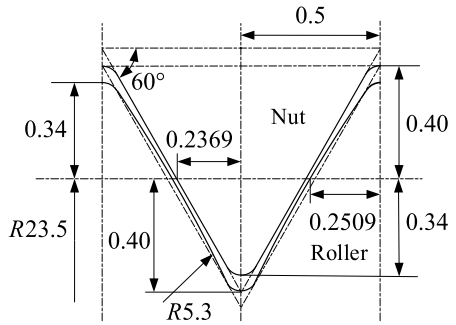

Figure 13 Cross-sectional view of the roller-nut engagement

nut. Therefore, reducing the radius of the roller arc can change the fit-up gap value between the arc and the beveled edge in the axis direction. Therefore, by moving the triangle and adjusting the radius of the roller arc, the problem of thread interference can be solved.

Since there are the convex platforms on the end surface of cam ring, it is necessary to ensure that the center surface of one of the convex platforms is on the same surface as the starting point of the nut thread when assembling the nut with cam ring. Meanwhile, the axial positions of the rollers relative to the carrier are different, so it is necessary to consider how to model in order to complete the corresponding assembly. The modeling and assembly principle is shown in Figure 14. Points S and $N^{'}$ are the starting points of the screw and nut threads, and are on their respective removal profile.

Since the roller tooth is grooved, it is necessary to ensure that the helix of nut is synchronized with that of the screw. As shown in Figure 14, both point S and point $N^{'}$ are on their thread pitch diameters and are spaced an integer multiple of the pitch from the end surface of the part. When the assembly is carried out, the reference planes of the screw and nut scanning profile are overlapped, and the phase angle between point S and point $N^{'}$ is 180°. The distance from point S to reference plane

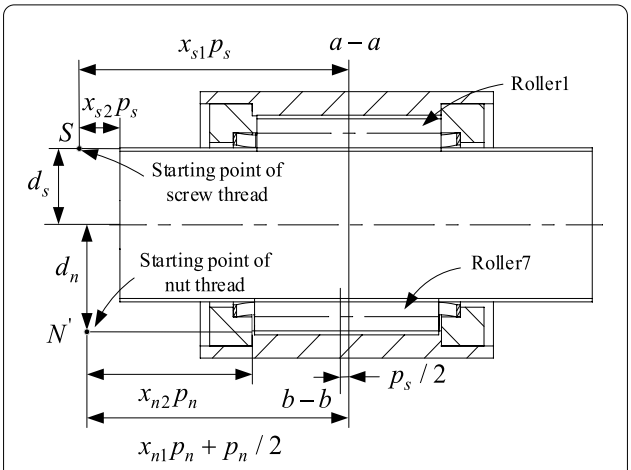

Figure 14 Diagram of screw and nut assembly relationships

$a-a$ is $x_{s1}p_s$, and the distance from point S to the end surface of the screw is $x_{s2}p_s$. Consequently, the distance between the screw's end surface and reference plane $a-a$ is set to $x_{s1}p_s - x_{s2}p_s$. Hereinto, x_{s1}, x_{s2}, x_{n1} and x_{n2} are arbitrary integers, and reference plane $a-a$ is the center surface of roller 1. The above operation can ensure that the screw/nut thread and the roller thread do not interfere with each other after the roller assembly is completed.

As one can see from Figure 14, the distance from point $N^{'}$ to the reference plane $a-a$ is $x_{n1}p_n + p_n/2$, which is increased by $p_n/2$ compared to point S. The main reason is that point S and roller 1 are in the same side of the central axis and the phase angle is zero, while the phase angle between point $N^{'}$ and point S is 180°.

3.2 RPRSM Virtual Assembly Method

Based on the special structure of the nut threadless area and the uniform circular distribution of the roller along the nut helix, the matching relationship should be paid attention to when assemble the RPRSM. The assembly method is as follows.

(1) In order to facilitate the roller assembly, it is necessary to ensure that the convex platform of cam ring is assembled in the correct position by first assembling the cam ring coaxially at one end of the nut. The position of the convex platform is fixed by adding overlap constraints to the nut reference plane $c_1 - c_1$ and cam ring reference plane $f-f$. That is, as shown in Figure 15, the convex platform of cam ring is on one side of the nut threadless area. Then, the other cam ring is installed at the other end of the nut with the convex platform positioned on the other side of the nut threadless area, and its refer-

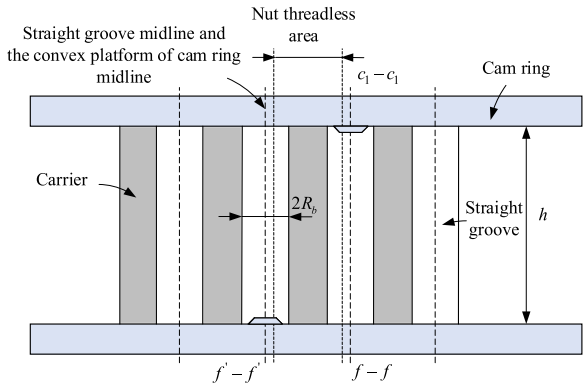

Figure 15 The assembly relation diagram of cam ring and carrier

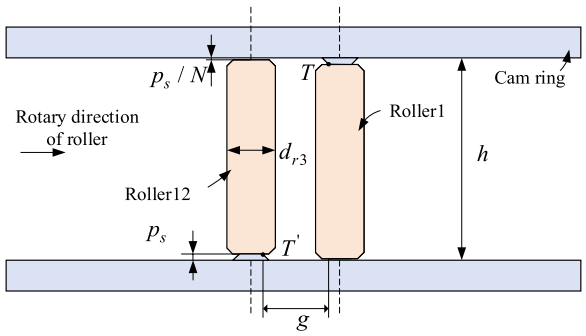

Figure 17 Both screw and nut are right-handed

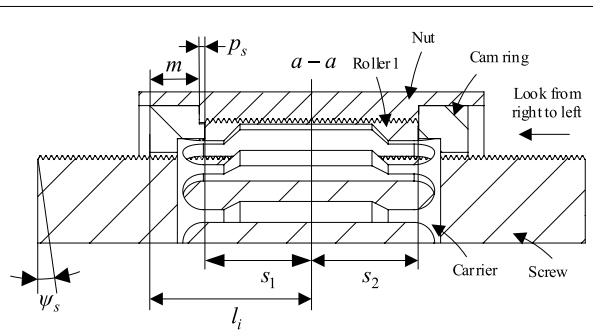

Figure 16 Cutaway view of roller assembly

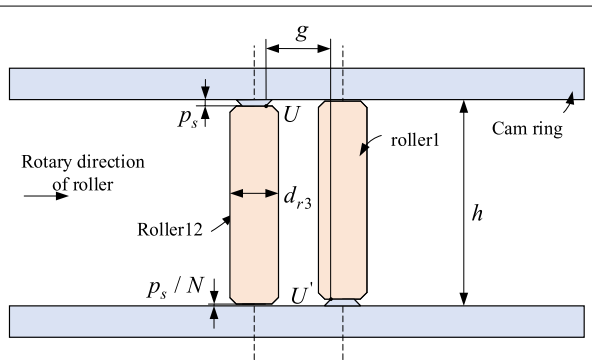

Figure 18 Both screw and nut are left-handed

ence plane $f^{'}-f^{'}$ is spaced $\varphi = 360°/N$ away from the reference plane $f-f$.

(2) The position relationship between the reference plane $a-a$ of roller 1 and the left end surface of the cam ring is shown in Figure 16. The distance of l_i is given by

$$l_i = m + s_1 + \frac{N-i-1}{N}p_s, \tag{34}$$

where s_1 is half of the roller length, N is the number of rollers, $i = 1,\ldots, N$, and l_i indicates the distance from the center surface of each roller to the left end surface of cam ring.

Combined with the assembly method, the RPRSM virtual assembly process based on the parameters in Table 1 is as follows.

(1) The cam ring should be placed appropriately according to the helical direction of screw and nut. As shown in Figures 17 and 18, the screw and the nut are both right-handed or left-handed, resulting in different layout of cam ring. Here-into, two cam ring spacing is expressed as $h = s_1 + s_2 + p_s/N + p_s$, and g is the distance between two convex platforms point T and point $T^{'}$. The roller major diameter d_{r3} needs to meet $d_{r3} < g$.

(2) One end of the nut is assembled coaxially with the cam ring, and the position of the convex platform of cam ring is on one side of the nut threadless area.

(3) As shown in Figure 15, the carrier must be positioned where the center line of one of the straight grooves coincides with that of the convex platform of cam ring. The other cam ring is installed with its convex platform positioned on the other side of the nut threadless area and is spaced $\varphi = 360°/N$ from the reference plane $f-f$.

(4) The roller 1 is inserted into the straight groove of the carrier, and one end of the roller should be close to the convex platform of cam ring while the roller groove should also engage with the nut, details are as follows.

① The distance between the center axis of the roller and the nut is 19.75 mm.

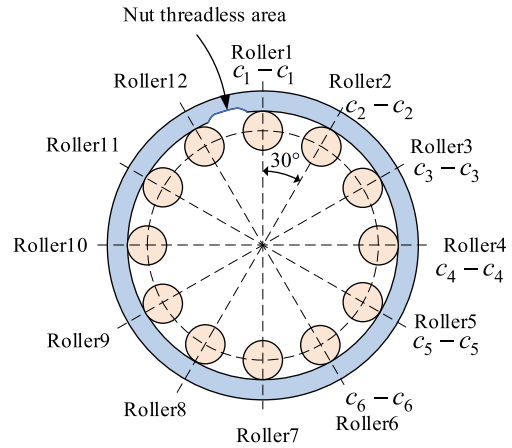

Figure 19 Roller assembly diagram

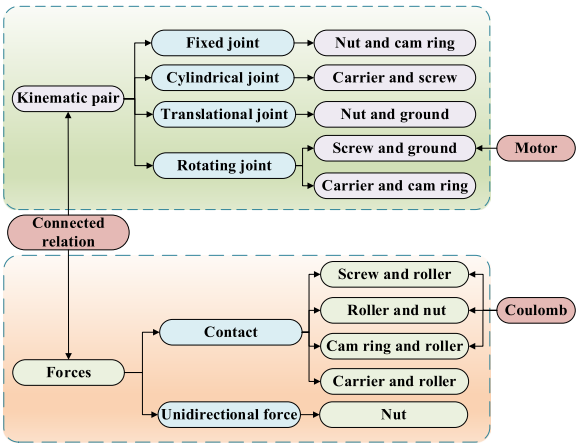

Figure 20 Basic connection relation of virtual prototype

② The reference plane over the center axis of the roller is overlapped with the corresponding reference plane $c_1 - c_1$ of the nut. Referring to Figure 16, the roller assembly diagram shown in Figure 19 can be obtained by viewing from the right to the left, and establish six reference planes over the axis of the nut, that is $c_i - c_i$, $i = 1, \ldots, N/2$.

③ The reference plane $a - a$ of roller 1 and the carrier reference plane $b_1 - b_1$ are overlapped. Therefore, the distance from the reference plane $a - a$ to the end surface of cam ring is l_1:

$$l_1 = m + s_1 + p_s. \tag{35}$$

(5) As shown in Figure 19, the roller 2 is also inserted into the straight groove of the carrier and is engaged with the nut thread, which is similar to the roller 1. In current case, the rollers are rotated 30°, and the end surface of roller 1 and roller 2 differ by a distance of p_s/N, that is, the distance from the center surface of roller 2 to the end surface of cam ring is l_2 :

$$l_2 = m + s_1 + \frac{N-1}{N} p_s. \tag{36}$$

(6) Referring to Figure 19, the remaining 10 rollers are installed clockwise to the carrier straight grooves in accordance with the above operation steps, and each roller rotation angle is also 30°. The distance l_i is:

$$\begin{cases} l_3 = m + s_1 + \frac{N-2}{N} p_s, \text{ roller3}, \\ \cdots\cdots \\ l_{12} = m + s_1 + \frac{N-11}{N} p_s, \text{ roller12}. \end{cases} \tag{37}$$

(7) After the roller, nut and cam ring are assembled, the starting point of the screw thread is in the same plane as that of the nut thread. That is, point S and point N' in Figure 13 are in the same plane, both the screw thread and the roller groove can be correctly assembled.

4 RPRSM Dynamic Simulation

4.1 Virtual Prototype Simulation Analysis Model

The basic connection relationship of RPRSM virtual prototype is shown in Figure 20. The specific process is as follows.

(1) Creating Constraints

The following constraints are added according to the RPRSM motion relationship: the nut maintains a relative position with the cam ring, imposing a fixed joint. The carrier and the screw move in relative rotary and linear motion, which a cylindrical joint is applied. The nut moves in a straight line, applying a translational joint between the nut and the ground. A rotating joint between the screw and the ground is applied, as well as a rotating joint between the carrier and cam ring.

(2) Load Applied

There're two types of contact forces: one is intermittent contact and the other is continuous contact. Adams/solver uses two calculation methods to calculate contact: restitution and impact. In this paper, the impact function method is used to calculate the contact, and the expression of the impact function is:

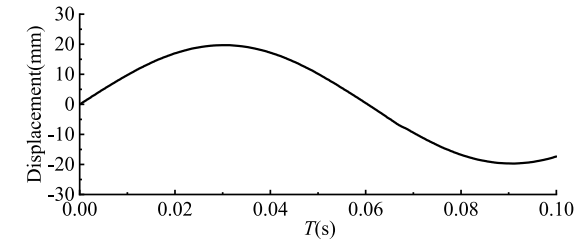

(a) Displacement of roller in x-axis direction

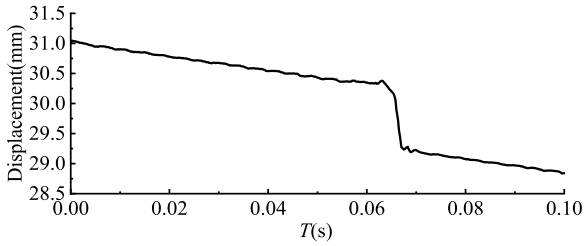

(b) Displacement of roller in z-axis direction

Figure 21 Displacement of roller

$$MAX\left\{0, K(q_0 - q)^e - C' \times \frac{dq}{dt} \times STEP(q, q_0 - d, 1, q_0, 0)\right\}, \tag{38}$$

where K is the stiffness coefficient; q is the distance variable between two points; q_0 is the reference distance between two objects to be in contact; e is the force index; C' is the maximum damping coefficient; t is the time; d is the penetration amount when the damping reaches its maximum value. That is, the penetration depth is used to prevent discontinuity of the damping condition during the collision.

The material of the main parts are set to GCr15, and the contact parameters are set as follows: The stiffness factor $K = 1\times10^5$ N/mm, force index $e = 1.5$, maximum damping factor $C = 50$ N·s/mm, and penetration depth $d = 0.1$ mm. The Coulomb method is used to consider the effect of friction, and the relevant parameters are set as follows: static coefficient $\mu_s = 0.3$, dynamic coefficient $\mu_d = 0.25$, static slip velocity $v_s = 900$ mm/s, and dynamic slip velocity $v_d = 1000$ mm/s.

4.2 Motion Relationship Analysis

Since the screw is the driving part, a constant speed 40π rad/s is applied in clockwise rotation (as shown in Figure 8). The simulation time is set to 0.1 s. The simulation results are shown in Figures 21, 22, 23, 24, 25. Since the twelve rollers are distributed uniformly in the circumferential direction, most of the results in this paper are represented with the simulation data of roller 7.

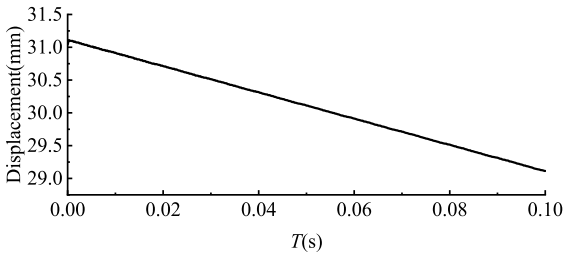

(a) Axial displacement of nut

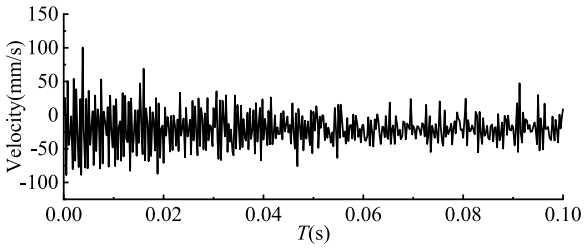

(b) Moving velocity of nut

Figure 22 Axial displacement and moving velocity of nut

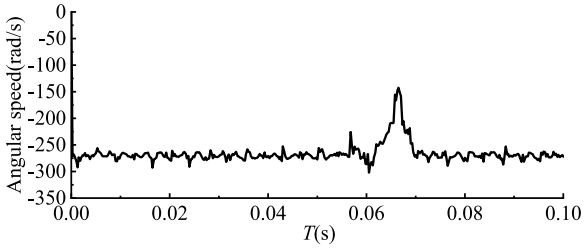

Figure 23 Angular speed of roller

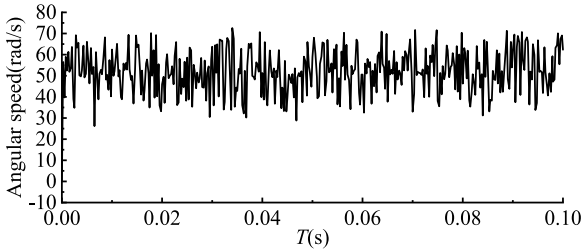

Figure 24 Angular speed of carrier

As can be seen from Figure 21, when the screw rotates 4π, the curve of roller displacement in x-axis direction is sinusoidal because of the roller's circle movement around the screw and the curve has about one-half cycle, and the corresponding time is known, so the orbital angle of roller is 1.62π. The roller completes the reset action

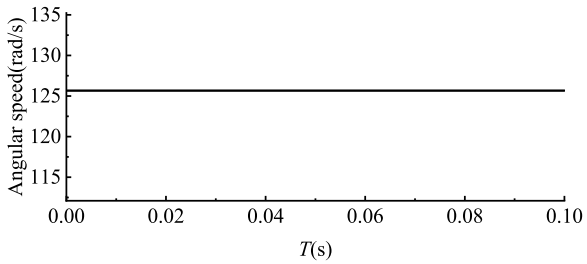

Figure 25 Angular speed of screw

near 0.07 s. The sudden change value is the screw pitch of 1 mm, and the roller moves the distance of 2.207 mm relative to the screw in 0.1 s. As one can see from Figure 21(b) and Figure 22(a), it can be observed that the translational velocity of roller is slower than that of nut by comparing the slope of two curves, mainly because the roller relative to the nut has a displacement in the opposite direction.

As can be seen from Figure 22, after two turns of the screw (0.1 s), the axial displacement of the nut is 1.996 mm, which is not equal to the displacement of roller. The mean value of the nut movement velocity $v_n = (-)19.79$ mm/s. The fluctuation of nut movement velocity v_n is larger than that of roller angular speed ω_r and carrier angular speed ω_c, mainly because of a small gap caused by the axial runout.

As shown in Figure 23, due to the small gap between the screw and the roller, the screw can be in contact with the roller after idling for a period of time. The average value of the roller angular speed $\omega_r = (-)$ 265.57 rad/s. During 0.06–0.07 s, the roller moves axially one pitch forward relative to the nut movement due to the role of the convex platform, so the roller angular speed has an abrupt change. When excluding the angular speed entering the nut threadless area during 0.06–0.07 s, the mean angular speed of the roller can be obtained as $\omega_r^{'} = (-)$ 268.98 rad/s.

As can be seen from Figures 24 and 25, the mean carrier angular speed is calculated as $\omega_c = 52.02$ rad/s, and the angular speed of screw is $\omega_s = 125.66$ rad/s. Referring to Figure 8, the roller angular speed is counterclockwise while the carrier and screw angular speed are clockwise, which is in accordance with the ± sign of the simulated angular speed.

The theoretical values of ω_r, ω_c, v_n, L_n and L_{r3} are known from Eqs. (23)–(33). They are compared with the simulated values and the errors are calculated, as listed in Table 2. Hereinto, the theoretical value of the roller angular speed $\omega_r^{'}$ in the nut thread area is the same as the roller angular speed ω_r.

As one can see from Table 2, the error between the theoretical and simulated values of each parameter is small

Table 2 Comparison between simulation value and theoretical value

	$\omega_r^{'}$(rad/s)	ω_c(rad/s)	v_n(mm/s)	L_n(mm)	L_{r3}(mm)
Theoretical value	− 268.08	50.9	− 20	2	2.19
Simulation value	− 268.98	52.02	− 19.79	1.996	2.207
Relative error	0.94%	2.20%	1.04%	0.20%	0.77%

and is less than 1%. The main reasons for the error are the existence of relative sliding between the screw/nut and the roller. The roller is grooved without end gear and has no spiral angle, only relying on the thread of the screw and nut to restrain its axial position. Besides, the screw/nut and the roller are affected by frictional force. In general, the simulated values of each parameter have small errors with their corresponding theoretical values, indicating that the simulation results of this paper are valid.

4.3 Effect of Different External Loads on Contact Force

Referring to the relevant technical manuals [30], the maximum load that RPRSM of this size can withstand is 60kN. Thus, 20, 40 and 60 kN are then selected to applied to the nut in the axial direction. Figures 26 and 27 show the contact force between the screw/nut and the roller in three directions. Figure 28 shows the average value of each roller contact force between the screw and the rol ler.

It can be markedly found from Figure 26(a) and (b), Figure 27(a) and (b) that there are positive and negative values of the contact force in x-axis and y-axis direction when the roller rotates. As shown in Figure 29, the directions of the contact force between the screw/nut and the roller change continuously along the circumferential direction of the screw.

Referring to Figures 26, 27 and 29, when the roller 7 begins to move, the contact forces between the screw/nut and the roller in x-axis are zero. Therefore, the roller has no angular acceleration and the carrier along the direction of the roller rotation will push the roller 7 to rotate. When the roller 7 moves after 0.03 s, the contact forces between the screw/nut and the roller in y-axis are zero. This is mainly because the screw is placed horizontally, and the roller is overhanging in the y-axis direction. At this moment, the roller is supported by the carrier in the y-axis direction, instead of the screw and nut. When the roller moves after 0.065 s, the roller will be reset. After 0.08 s, the contact forces in x-axis and y-axis are not zero, so the roller has the angular acceleration caused by friction. The moment at 0.09 s is similar to that of 0.03 s with the contact forces in y-axis being zero.

From Figures 26(c) and 27(c), it can be observed that the contact forces between the screw/nut and the roller

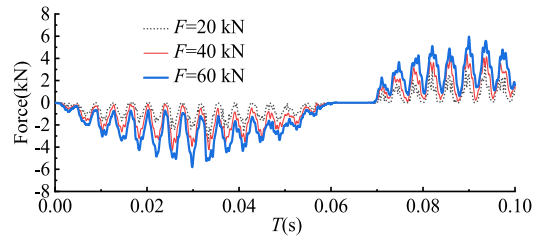

(a) Contact force between screw and roller in *X* axis

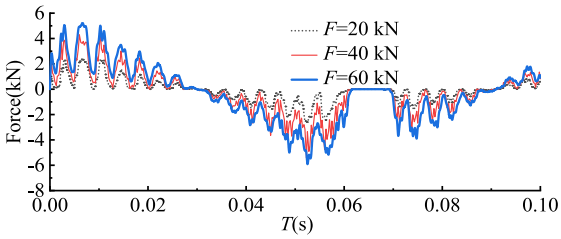

(b) Contact force between screw and roller in *Y* axis

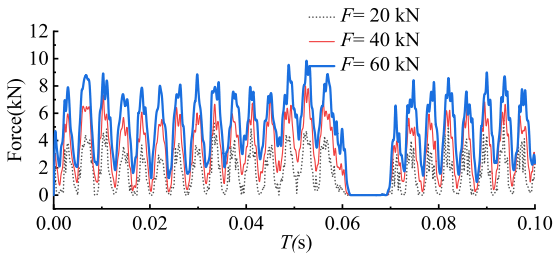

c) Contact force between screw and roller in *Z* axis

Figure 26 Contact force curve between screw and roller

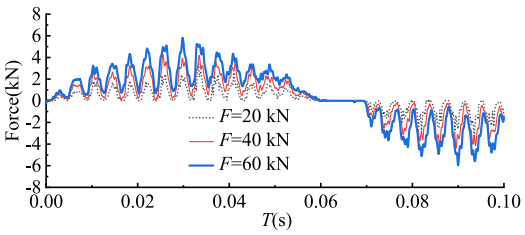

(a) Contact force between nut and roller in *X* axis

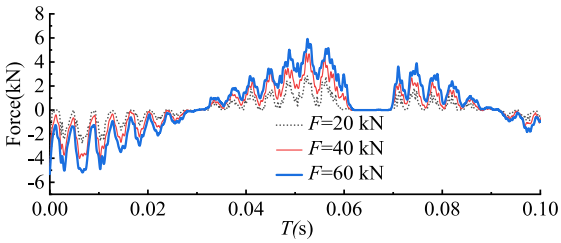

(b) Contact force between nut and roller in *Y* axis

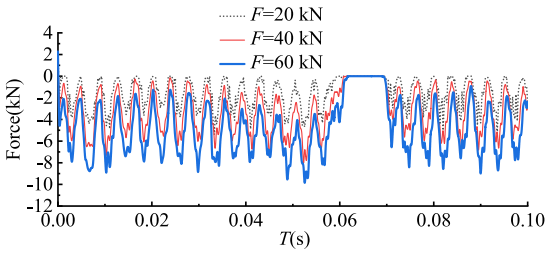

(c) Contact force between nut and roller in *Z* axis

Figure 27 Contact force curve between nut and roller

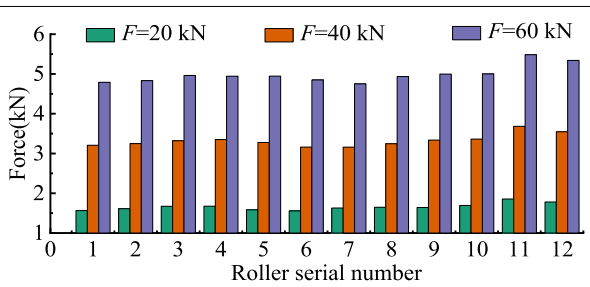

Figure 28 Average contact force of each roller on *z* axis between screw and roller

are intermittent. The peak value increases with the increase of the external load. When the contact force reaches the peak, the roller pushes the carrier for circular motion, that is, the roller collides with the carrier in a certain direction. Then the roller separates from the carrier, so the contact force slowly decreases until it reaches the minimum value. After that, the roller collides with the carrier in the other direction until the contact force reaches the peak. Therefore, the contact force cycle shows the sine curve characteristic. After 0.06 s, the roller enters the nut threadless area, and the roller is disengaged from the screw by the convex platform, thus completes the reset action across the screw thread. At the same time, the contact forces between the screw/nut and the roller are also zero since the roller loses the nut thread restraint.

As can be seen from Figure 28, the contact forces between the roller 1 to 10 and the screw under different loads are similar in size. The contact force of the roller 11 and 12 is slightly larger, mainly because the roller rotation angle has not reached one turn, and the roller 11 and 12 have not entered into the nut threadless area. The average contact forces between the screw and the roller are summed up under three loads to obtain $F_{sum1} = 19.91$ kN, $F_{sum2} = 39.90$ kN and $F_{sum3} = 59.83$ kN. The relative errors are 0.45%, 0.25% and 0.43% compared to the initial external load, which are both less than 1%, thus proving the accuracy of the simulation.

Figures 30, 31, 32 show the collision forces between the roller 7 and the cam ring under three loads, the collision

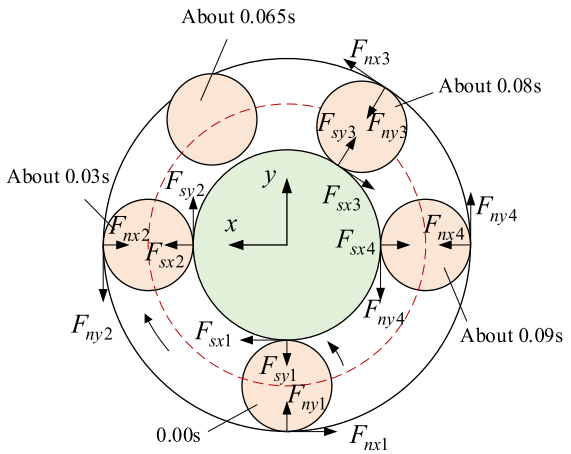

Figure 29 Contact force analysis of roller 7 during 0.1 s

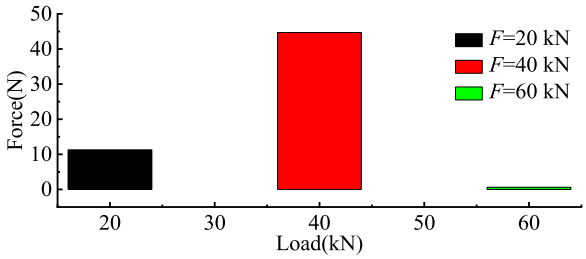

Figure 30 Collision force between roller 7 and cam ring under three loads

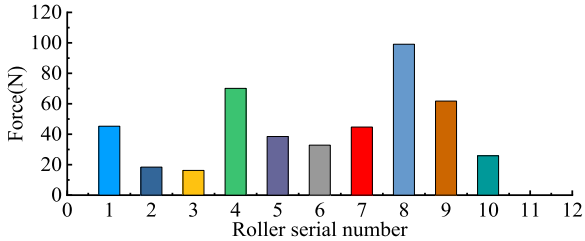

Figure 31 Collision force between roller and cam ring at $F = 40$ kN

force between the twelve rollers and the cam ring at $F = 40$ kN, and the collision forces variation between the roller and the carrier under three loads, respectively.

As can be seen from Figure 30, when external load $F = 40$ kN, the roller just collides with the cam ring, and the collision force is 44.70 N, followed by 11.30 N when $F = 20$ kN, and when $F = 60$ kN, the collision force is 0.63 N. Besides, it can be seen from Figure 31 that the collision forces between cam ring and different rollers are random because of the dynamic operation of RPRSM. By analyzing the collision force of the same roller 7 under three different loads and that of different rollers under the same external load, the impact of collision force on the RPRSM operation accuracy is negligible because the collision force fluctuation range is small compared to the external load.

As shown in Figure 32, in the certain period of 0.1 s, the roller is oscillating in the straight groove of the carrier. The main reason is that there is a small gap between the roller and the straight groove of the carrier. By analyzing the collision forces under $F = 20$ kN, $F = 40$ kN and $F = 60$ kN, it can be seen that the higher load applied, the higher peak collision force appears. However, there is a moment of small collision force even when the larger load is applied. The main reason is that there is relative sliding between the screw/nut and the roller when the motion is transferred.

5 Conclusions

Based on the fact that the rollers cross the screw thread teeth by the convex platform of cam ring, the equations related to the dimensional parameters of the nut threadless area is derived. The design case of roller, screw and nut cross-section profile is constructed, and the meshing accuracy of the screw/nut and roller threads can be improved by adjusting the gap between the two beveled edges and that between the arc and the beveled edge. To ensure the effective assembly of RPRSM, the relationship between the distances from the center surface of different rollers to the end surface of cam ring is given. On this basis, the motion characteristics of RPRSM are simulated and compared with the theoretical results to verify the correctness of the simulation. Finally, the contact forces and collision forces between different parts are calculated after applying different loads to the nut, respectively. The main conclusions are summarized as follows.

(1) When the roller moves in a circular motion and enters into the nut threadless area, there is sliding friction between its end face and the convex platform of cam ring, so the angular speed of the roller drops sharply. By adjusting the coefficient of dynamic friction between the roller and the convex platform of cam ring, the influence on RPRSM accuracy can be reduced.
(2) The contact force between the screw/nut and the roller shows a sine curve characteristic in the operational cycle, mainly due to the small gap between the carrier and the roller.
(3) The peak of collision force between the roller and the cam ring is not affected by the size of load, and the collision force between the roller and the carrier increases with the increase of external load.

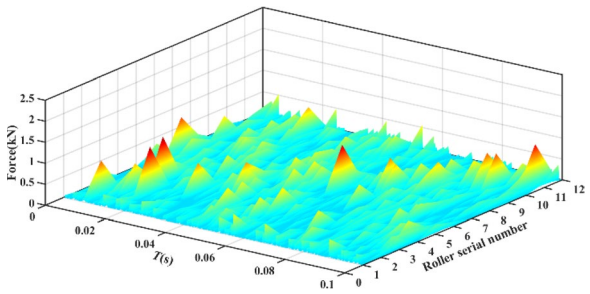

(a) Collision force between rollers and carrier at F=20 kN

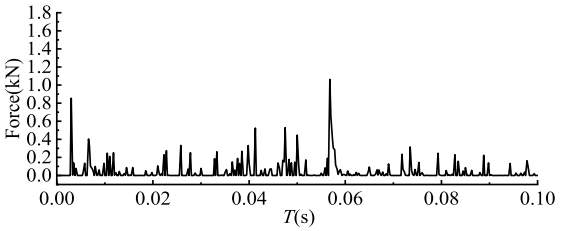

(b) Collision force between roller7 and carrier at F=20 kN

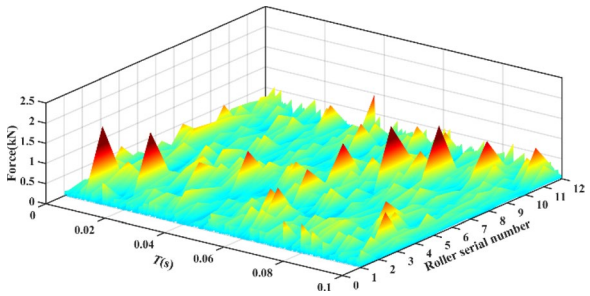

(c) Collision force between rollers and carrier at F=40 kN

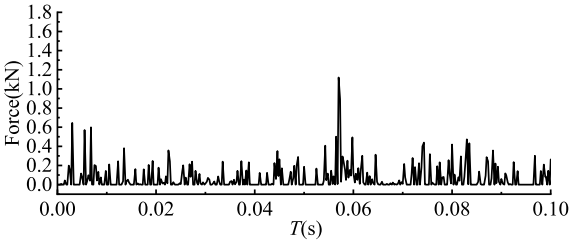

(d) Collision force between roller7 and carrier at F=40 kN

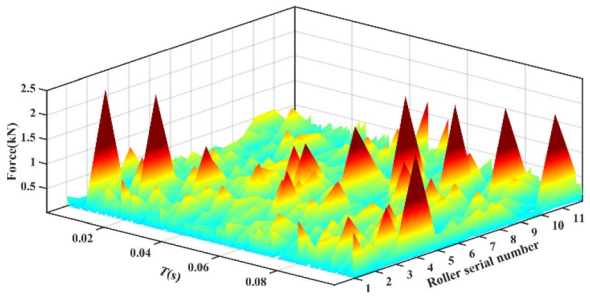

(e) Collision force between rollers and carrier at F=60 kN

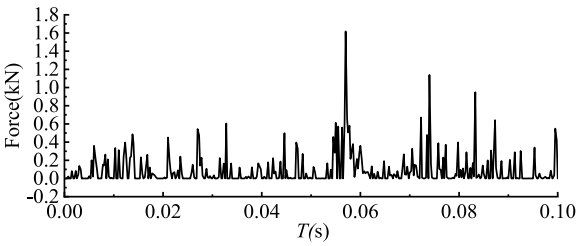

(f) Collision force between roller7 and carrier at F=60 kN

Figure 32 Collision force variation between rollers and carrier under three loads

Acknowledgements
Not applicable.

Author Contributions
GQ and RL wrote the manuscript; SG established the assembly method; ZS and SM assisted with English writing and dynamic simulation analyses. All authors read and approved the final manuscript.

Authors' Information
Guan Qiao, born in 1990, is currently an associate professor at *Inner Mongolia University of Technology, China*. His main research interests include planetary roller screw mechanism design and transmission characteristic analysis.
Rong Liao, born in 1996, is currently a master candidate at *Inner Mongolia University of Technology, China*. His main research interests include recirculating planetary roller screw mechanism design and dynamic analysis.
Shijie Guo, born in 1985, is currently an associate professor at *Inner Mongolia University of Technology, China*. His main research interests include geometric accuracy enhancement of five-axis machine tool.
Zhenghong Shi, born in 1983, is currently an engineer at *University of Cincinnati, USA*. His main research interests include vibration analysis and tribology of gear transmission.
Shangjun Ma, born in 1980, is currently an associate professor at *Northwestern Polytechnical University, China*. His main research interests include planetary roller screw mechanism design and test analysis.

Funding
Supported by National Natural Science Foundation of China (Grant Nos. 52065053, 51875458), Natural Science Foundation of Inner Mongolia (Grant No. 2020BS05003), and Inner Mongolia Science and Technology Project (Grant No. 2020GG0288).

Competing Interests
The authors declare no competing financial interests.

Author Details
[1]Inner Mongolia Key Laboratory of Advanced Manufacturing Technology, Inner Mongolia University of Technology, Hohhot 010051, China. [2]University of Cincinnati, Cincinnati, OH 45221, USA. [3]Shaanxi Engineering Laboratory for Transmissions and Controls, Northwestern Polytechnical University, Xi'an 710072, China.

Received: 7 March 2022 Revised: 3 May 2022 Accepted: 17 June 2022
Published online: 07 July 2022

References

[1] G Qiao, G Liu, Z H Shi, et al. A review of electromechanical actuators for more/all electric aircraft systems. *Proceedings of the Institution of Mechanical Engineers Part C-Journal of Mechanical Engineering Science*, 2018, 232(22): 4128–4151.
[2] F Lisowski. The specific dynamic capacity of a planetary roller screw with random deviations of a thread pitch. *Journal of Theoretical and Applied Mechanics*, 2017, 55(3): 991–1001.
[3] Y Q Liu, Y Shang, J S Wang. Mathematical analysis of the meshing performance of planetary roller screws applying different roller thread shapes. *Advances in Mechanical Engineering*, 2017, 9(5): 1–11.
[4] X J Fu, G Liu, S J Ma, et al. An efficient method for the dynamic analysis of planetary roller screw mechanism. *Mechanism and Machine Theory*, 2020, 150: 1–15.
[5] A Andrade, D Nicolosi, J Lucchi, et al. Auxiliary total artificial heart: a compact electromechanical artificial heart working simultaneously with the natural heart. *Artificial Organs*, 1999, 23(9): 876–880.
[6] S A Velinsky, B Chu, T A Lasky. Kinematics and efficiency analysis of the planetary roller screw mechanism. *Journal of Mechanical Design*, 2009, 131(1): 1–8.
[7] J-C Maré, J Fu. Review on signal-by-wire and power-by-wire actuation for more electric aircraft. *Chinese Journal of Aeronautics*, 2017, 30(3): 857–870.
[8] J Meng, X Du, Y Li, et al. A multiscale accuracy degradation prediction method of planetary roller screw mechanism based on fractal theory considering thread surface roughness. *Fractal and Fractional*, 2021, 5(4): 1–20.
[9] L Zu, Z Zhang, L Gao. Design and bearing characteristics of planetary roller screws based on aerospace high-load conditions. *Advances in Mechanical Engineering*, 2018, 10: 1–11.
[10] Y Liu, J Wang, H Cheng, et al. Kinematics analysis of the roller screw based on the accuracy of meshing point calculation. *Mathematical Problems in Engineering*, 2015: 1–10.
[11] X Li, G Liu, X J Fu, et al. Lagrange-method-based dynamic analysis of multi-stage planetary roller screw mechanism. *Mechanical Sciences*, 2021, 12(1): 471–478.
[12] S Sandu, N Biboulet, D Nelias, et al. Analytical prediction of the geometry of contact ellipses and kinematics in a roller screw versus experimental results. *Mechanism and Machine Theory*, 2019, 131: 115–136.
[13] G Qiao, G Liu, S J Ma, et al. Thermal characteristics analysis and experimental study of the planetary roller screw mechanism. *Applied Thermal Engineering*, 2019, 149: 1345–1358.
[14] W J Zhang, G Liu, S J Ma, et al. Load distribution over threads of planetary roller screw mechanism with pitch deviation. *Proceedings of the Institution of Mechanical Engineers, Part C: Journal of Mechanical Engineering Science*, 2019, 233(13): 4653–4666.
[15] W J Zhang, G Liu, R T Tong, et al. Load distribution of planetary roller screw mechanism and its improvement approach. *Proceedings of the Institution of Mechanical Engineers, Part C: Journal of Mechanical Engineering Science*, 2016, 230(18): 3304–3318.
[16] S J Ma, G Liu, R T Tong, et al. A new study on the parameter relationships of planetary roller screws. *Mathematical Problems in Engineering*, 2012: 1–29.
[17] F Lisowski, J Ryś. A methodology of designing the teeth conjugation in a planetary roller screw. *Archive of Mechanical Engineering*, 2016, 63(4): 589–603.
[18] F Lisowski. Optimization of thread root undercut in the planetary roller screw. *Czasopismo Techniczne*, 2017(9): 219–227.
[19] C-K Shih, C Hung, R-Q Hsu. The finite element analysis on planetary rolling process. *Journal of Materials Processing Technology*, 2001, 113(1): 115–123.
[20] S J Ma, G Liu, J X Zhou, et al. Optimal design and contact analysis for planetary roller screw. *Applied Mechanics and Materials*, 2011, 86: 361–364.
[21] F Abevi, A Daidie, M Chaussumier, et al. Static load distribution and axial stiffness in a planetary roller screw mechanism. *Journal of Mechanical Design*, 2016, 138(1): 1–11.
[22] X J Fu, G Liu, X Li, et al. Dynamic modeling of the double-nut planetary roller screw mechanism considering elastic deformations. *Journal of Computational and Nonlinear Dynamics*, 2021, 16(5): 1–13.
[23] X J Fu, G Liu, S J Ma, et al. Kinematic model of planetary roller screw mechanism with run-out and position errors. *Journal of Mechanical Design*, 2018, 140(3): 1–10.
[24] S J Ma, T Zhang, G Liu, et al. Kinematics of planetary roller screw mechanism considering helical directions of screw and roller threads. *Mathematical Problems in Engineering*, 2015: 1–11.
[25] G Qiao, G Liu, S J Ma, et al. Dynamic characteristic analysis for an electromechanical actuator based on planetary roller screw mechanism. *Journal of Vibration and Shock*, 2016, 35(7): 82–88, 101. (in Chinese)
[26] M H Jones, S A Velinsky. Kinematics of roller migration in the planetary roller screw mechanism. *Journal of Mechanical Design*, 2012, 134(6): 1–6.
[27] Y Hojjat, M M Agheli. A comprehensive study on capabilities and limitations of roller-screw with emphasis on slip tendency. *Mechanism and Machine Theory*, 2009, 44(10): 1887–1899.
[28] S J Ma, T Zhang, G Liu, et al. Bond graph-based dynamic model of planetary roller screw mechanism with consideration of axial clearance and friction. *Proceedings of the Institution of Mechanical Engineers, Part C: Journal of Mechanical Engineering Science*, 2018, 232(16): 2899–2911.
[29] C F Zou, H J Zhang, J Zhang, et al. Acceleration-dependent analysis of vertical ball screw feed system without counterweight. *Chinese Journal of Mechanical Engineering*, 2021, 34(1): 1–13.
[30] ROLLVIS SWISS. *Satellite roller screws catalogue 2019*. Switzerland, ROLLVIS SA, 2019[2022-05-02]. https://rollvis.com/wpcontent/uploads/2021/09/Catalogue-EN-2018-compressed.pdf.